SUPPLEMENTARY MATERIALS

Methods

Light- and Scanning Electron Microscopy. The petrography and microstructure of the ultramylonite have been investigated with polarized light- and scanning electron microscopy on polished thin sections cut perpendicular to the foliation and parallel to the stretching lineation. SEM backscatter electron images were collected with a Jeol-840 SEM at the Department of Medical Biology, University of Tromsø, and with a Philips XL-30 FEG-ESEM at the Department of Geological Sciences, Stockholm University. The same thin sections were used for electron backscattered diffraction (EBSD). The grain size and aspect ratio of individual grains were measured on grain boundary maps obtained from manually digitizing SEM-BSE and EBSD images. The 2D size of the grains was calculated as the diameter of the circle with an area equivalent to that of the grain using the freeware Image SXM software (http://www.ImageSXM.org.uk).

EBSD and EDS Analysis. EBSD and EDS analysis were carried out on a Jeol LV6610 SEM equipped with an Oxford Instruments Nordlys Nano EBSD detector and with an Oxford Instruments SDD X-Max 80 mm^2 EDS detector at the Electron Microscopy Centre of Plymouth University. Additional EBSD analysis was conducted on a Philips XL-30 FEG-ESEM equipped with a HKL Technology (Oxford Instruments) Nordlys detector at the Department of Geological Sciences, Stockholm University. Thin sections were chemically polished carbon coated (for EBSD analysis in Plymouth) or left uncoated (for the EBSD analysis in Stockholm) during the acquisition of the electron backscatter patterns over gridded areas of varying sizes. Step sizes of 1, 2 and 3 μm were used in the 3 EBSD datasets presented in this study. Working conditions during the pattern acquisition were 20 or 25 keV accelerating voltage and either low vacuum (0.3-0.4 torr: Stockholm) or high vacuum (Plymouth). EBSD patterns were indexed and processed with the Channel 5 analysis suite from HKL Technology (Oxford Instruments). A match unit for oligoclase was created with the Twist component of the Channel 5 suite using the cell parameters for An16 (spatial group C-1) reported in Phillips et al. (1971) and served as theoretical model to index plagioclase. Noise reduction on the raw EBSD data was performed following the procedure tested by Prior et al. (2002) and Bestmann and Prior (2003). Crystallographic data were plotted on pole figures (upper hemispheres) using one point per grain.

X-Ray Microtomography. Microtomographic samples with a diameter of 1 mm were extracted from the ultramylonite sample shown in Fig. DR1B using a rock drill. These samples were scanned at the microtomography beamline 2BM of the Advanced Photon Source (USA). A double multilayer monochromator of 1.5% band- width provided 27 KeV X-rays; radiographic projections were collected in transmission mode by a CCD camera behind the sample in the hutch configuration. The sample detector distance was 70 mm. During each scan, 1440 projections were collected through rotating the samples in steps of 0.125° over 180°. The acquisition time for each data set was about 25 min. From the radiographic projections, three-dimensional absorption microtomography datasets were reconstructed using filtered back-projection.

Two microtomographic data-sets (Lu-1_light and Lu-3_light) were cropped to a volume of 1000x1000x750 voxels, which corresponds to 650x650x488 μm. From these subvolumes, pores, which are the least-attenuating, hence darkest phase in the data, were segmented by binary thresholding. From the same raw data, micas were segmented using the same algorithm. Biotite was chosen because it defines the mylonitic foliation in the sample. From the segmented mica data artefacts (mostly phase contrast 'shadows') had to be manually removed. Binary data of both the pores and the micas were sequentially loaded into Blob3D (Ketcham, 2005) for analysis. Blob3D recognises face-connected voxels of the same kind as clusters (or 'blobs'), which allows determining for each cluster the volume, shape, location and orientation (given in direction cosine of the inscribed eigenvectors), amongst other parameters. For our orientation analysis, all clusters smaller than 34 μm^3 (125 voxels) and larger than 4120 μm^3 (15000 voxels) were discarded. The former would have introduced artefacts due to the limited possibilities to arrange a small number of voxels in a pore cluster, and the latter would have very complex shapes, producing meaningless results. We furthermore discarded pore clusters with aspect ratios ≤ 1.7 and mica clusters with aspect ratios < 3. The orientation values of the longest eigenvector were converted into dip direction/dip angle values using the formulation given in Groshong (2008).

For each of the two datasets (Lu-1_light and Lu-3_light), two orientation datasets exist – one for the mica grains and one for the pores. The longest eigenvectors of both mica data-sets cluster around well-defined maxima. We assume these maxima to define the orientation of the longest diameter of the finite strain ellipsoid in each sample. As can be seen in the supplementary movies and also Fig. 3A, the mica furthermore define a mylonitic foliation. We used these two orientations as a kinematic framework. Because this framework does not

spatially coincide with the Cartesian coordinate axes of the microtomography data, we rotated the maximum defined by the longest eigenvectors of the mica data into a horizontal E-W orientation and the pole to the foliation in a horizontal N-S orientation using Stereo32 (Fig. 3A and DR2). The exact same rotations were then applied to the longest eigenvectors of the Lu-3_light and Lu-1_light pore populations, which yield the stereo plots shown in Fig. 3B and DR2. This allowed us to assess the orientation of the pores in a kinematic context.

Whole-Rock Chemical Analysis. Whole-rock chemical analysis of major elements was performed by wavelength dispersive X-Ray fluorescence (WD-XRF) analysis with a Bruker S8 Tiger XRF spectrometer at the Department of Geology, University of Tromsø. Powder samples were mixed and diluted at 1:7 with $Li_2B_4O_7$ flux, and melted into fused beads. Loss on ignition (LOI) was determined from weight lost after ignition at 1050°C for 1.5 h. Total Carbon (TC) was measured with a LECO CS-200 at the Department of Geology, University of Tromsø. The LECO CS-200 uses infrared absorption to measure the quantity of carbon dioxide generated by combustion of the sample in an induction furnace in a pure oxygen environment. Accuracy of the measurements is ± 2 ppm.

Supplementary Information on the Mass-Balance Calculations

The two samples were collected along a continuous strain gradient in the field at a relative distance of 1 meter, so that we can safely conclude that the ultramylonite derives from (micro)structural and mineralogical modifications of the monzonite. The mass-balance calculations were carried out following the method designed by Potdevin and Marquer (1987), which is referred to as the 'normalized Gresens' method. The method uses the following equation to derive mass gain or loss of a chemical component n during modification of rock A to rock B in relationship to the initial amount of the component n in rock A:

$$\Delta X_n = F_v\,(\rho_B/\rho_A)(X_{nB}/X_{nA}) - 1 \qquad (1)$$

ΔXn represents the gain or loss of chemical component n related to its initial content in rock A, F_v is the volume factor (F_v = V modified rock B/V initial rock A), X_{nA} is the weight % of the component n in the initial rock A, X_{nB} is the weight % of the component n in the modified rock B, ρ_A is the density of the initial rock A, and ρ_B is the density of the modified rock B. Our calculations refer to the transformation protolith → ultramylonite (sample LST29F → sample LST29B). The main differences are in the LOI and TC content, consistent with fluid infiltration during shear zone formation. The very minor difference between the compositions

of the monzonite and ultramylonite (Table DR1) indicate that, apart form the fluid infiltration, there has been no major chemical change during deformation. Our whole-rock chemical composition data are consistent with the average composition of the Raftsund mangerite (Griffin et al. 1978). Thus, we are confident that primary heterogeneities of the protolith do not represent a limitation to our analysis.

The density of the samples have been measured with a pycnometer using pulverized material at the Department of Geology, University of Tromsø, following routine procedures outlined in Hutchinson (1975). Weight measurements were repeated 5 times for each sample, and were reproducible with an accuracy of ± 0.004 grams. The densities of the protolith (monzonite) and of the ultramylonite are 2.711 g/cm^3 and 2.654 g/cm^3, respectively.

Setting ΔX_n for TC = 2.75 and solving (1) for F_v, we obtain F_v = 1.023. This means a 2.3% volume increase. Setting F_v = 1.023 and solving (1) for ΔXn, we derive the following gains or losses of chemical components:

	F_v	ΔXn
SiO_2	1.023	0.0150
Al_2O_3	1.023	0.0264
TiO_2	1.023	- 0.2642
Cr_2O_3	1.023	- 0.3932
Fe_2O_3	1.023	- 0.1644
MnO	1.023	0.1133
MgO	1.023	- 0.1416
CaO	1.023	- 0.0991
Na_2O	1.023	0.1741
K_2O	1.023	- 0.1472
P_2O_5	1.023	- 0.2025
LOI	1.023	1.7635
TC	1.023	2.7500

REFERENCES CITED

Bestmann, M., and Prior, D.J., 2003, Intragranular dynamic recrystallization in naturally deformed calcite marble: diffusion accommodated grain boundary sliding as a result of subgrain rotation recrystallization: Journal of Structural Geology, v. 25, p. 1597-1613.

Griffin, W.L., Taylor, P.N., Hakkinen, J.W., Heier, K.S., Iden, I.K., Krogh, E.J., Malm, O., Olsen, K.I., Ormaasen, D.E., and Tveten, E., 1978, Archaean and Proterozoic crustal

evolution in Lofoten-Vesterålen, N Norway: Journal of the Geological Society [London], v. 135, p. 629-647.

Groshong, R.H., 2008, 3D Structural Geology - A practical guide to quantitative surface and subsurface map interpretation. Springer, 400 pp.

Hutchinson, C.S., 1975, Laboratory handbook of petrographic techniques: Wiley, New York, 527 p.

Ketcham, R.A., 2005, Computational methods for quantitative analysis of three-dimensional features in geological specimens: Geosphere, v. 1, p. 32-41.

Phillips, M.V., Colville, A.A., and Ribbe, P.H., 1971, The crystal structures of two oligoclases: a comparison with low and high albite: Zeitschrift für Kristallographie, v. 133, p. 43-65.

Potdevin, J.L., and Marquer, D., 1987, Méthodes de quantification des transferts de matière par les fluides dans les roches métamorphiques déformées: Geodinamica Acta, v. 1, p. 193-206.

Prior, D.J., Wheeler, J., Peruzzo, L., Spiess, R., and Storey, C., 2002, Some garnet microstructures: an illustration of the potential of orientation maps and misorientation analysis in microstructural studies: Journal of Structural Geology, v. 24, p. 999-1011.

Table DR1. Whole-rock chemical composition (major elements) of the protolith (LST29F) and of the ultramylonite (LST29B) samples used for the mass-balance calculations.

Label	**LST29F**	**LST29B**
Rock Type	Undeformed Monzonite	Ultramylonite
SiO_2	58.61	58.97
Al_2O_3	18.67	18.99
TiO_2	1.04	0.76
Cr_2O_3	0.01	0.01
Fe_2O_3	5.24	4.34
MnO	0.09	0.10
MgO	0.98	0.84
CaO	3.86	3.45
Na_2O	5.19	6.04
K_2O	4.72	3.99
P_2O_5	0.49	0.39
Total	98.90	97.86
LOI	0.207	0.567
TC	0.037	0.138

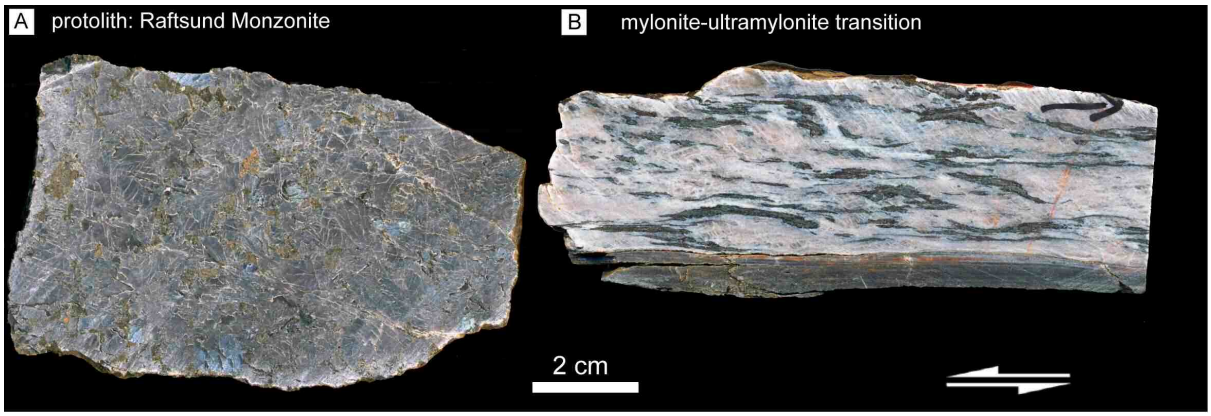

Figure DR1. Hand specimens of the monzonite protolith (A) and of the mylonite-ultramylonite transition (B).

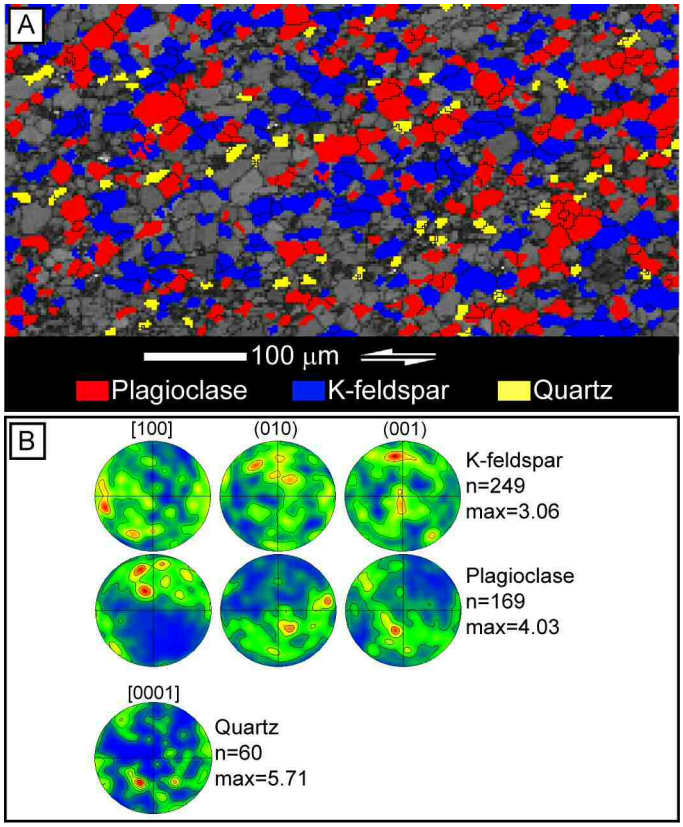

Figure DR2. A: EBSD-derived phase map of part of the same feldspathic layer shown in Fig. 2A of the paper. Note the festoons of quartz grains with a C'-band orientation for a sinistral sense of shear. B: Pole figures of K-feldspar, plagioclase and quartz grains in A.

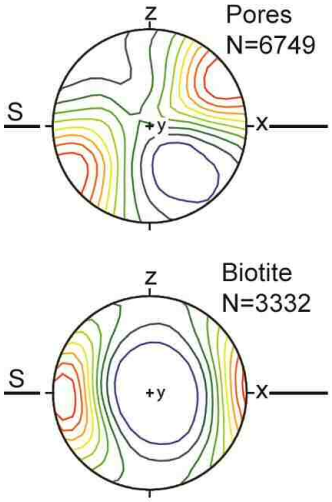

Figure DR3. Synchrotron x-ray microtomographic data Lu-1_light (compare with Fig. 3B). S is the trace of the ultramylonite foliation, Z is the pole to the foliation, X is parallel to the stretching lineation. Pole figure illustrating the long axes of pores preferentially oriented at 20-30° to the foliation (top) and the preferred orientation of biotite long axis aligned in the

foliation plane (bottom). Equal area lower hemisphere stereoplots. Contouring is up to 10 times MUD.

Movie DR_Lu-1_pores_slcmigration. Migrating slice through the microtomographic data-set Lu-1_light (volume of 650x650x488 μm). Grey values correspond to x-ray absorption. See text for further details.

Movie DR_Lu-3_pores_slcmigration. Thick migrating slice through the microtomographic data-set Lu-3_light (volume of 650x650x488 μm). Grey values correspond to x-ray absorption. Red=biotite, yellow=pores. The greyscale image is the backside of a thin migrating box through the 3D data-set, in which pores and biotite are highlighted. As the box moves through the volume, pores and biotite disappear out of the box at the front and enter the slice at the back, through the greyscale image See text for further details.